Clim. Past Discuss., 10, 3989–4032, 2014
www.clim-past-discuss.net/10/3989/2014/
doi:10.5194/cpd-10-3989-2014

Climate of the Past Discussions
Open Access

Atmospheric circulation controls on the inter-annual variability in precipitation isotope ratio in Japan

N. Kurita[1], Y. Fujiyoshi[2], T. Nakayama[3], Y. Matsumi[3], and H. Kitagawa[1]

[1]Graduate School of Environmental Studies, Nagoya University, Furo-cho, Nagoya, 464-8601, Japan
[2]Institute of Low Temperature Science, Hokkaido University, Kita-19 Nishi-8, Sapporo, 060-0819, Japan
[3]Solar-Terrestrial Environment Laboratory, Nagoya University, Furo-cho, Nagoya, 464-8601, Japan

Received: 27 August 2014 – Accepted: 9 September 2014 – Published: 2 October 2014

Correspondence to: N. Kurita (kurita.naoyuki@e.mbox.nagoya-u.ac.jp)

Published by Copernicus Publications on behalf of the European Geosciences Union.

Abstract

This study explored the primary driver of variations of precipitation isotopes at multiple temporal scales (event, seasonal and inter-annual scales) to provide a greater depth of interpretation for isotope proxy records in Japan. A one-year record of the isotopic composition of event-based precipitation at Nagoya in central Japan showed less seasonal variation, but there is large isotopic variability on a storm-to-storm basis. In the summer, southerly flows transport isotopically enriched moisture from subtropical marine regions with the result that the rainfall produced by the subtropical air, or warm rainfall, was relatively enriched in heavy isotopes in comparison with the other rainfall events. In the winter, storm tracks are the dominant driver of storm-to-storm isotopic variation, and relatively lower isotopic values occurred when northerly winds in association with extratropical cyclones passing off the south coast of Japan (Nangan cyclone) brings cold precipitation. Using the historical 17 year record of monthly isotopes in precipitation at Tokyo station, we explored if the factors controlling event-scale isotopic variability can account for inter-annual isotopic variability. The relatively higher isotopes in summer precipitation were attributed to the higher contribution of the warm rainfall to the total summer precipitation. On the other hand, year-to-year variation of isotopic values in winter precipitation was negatively correlated with the relative ratio of the Nangan cyclone rainfall to the total winter precipitation. The 17 year precipitation history demonstrates that event-scale isotopic variability related to changes in meridional moisture transport is the primary driver of inter-annual isotopic variability in winter and summer precipitation. The meridional moisture transport to central Japan is likely linked to the activity of the western North Pacific subtropical high in summer and the intensity of the East Asian winter monsoon in winter. Therefore, isotope-based proxy records archived in central Japan may enable us to examine past atmospheric circulation changes in East Asia in response to climate variability.

CPD
10, 3989–4032, 2014

1 Introduction

The hydrogen and oxygen isotope records preserved in natural archives such as speleothems, tree ring cellulose, leaf wax, lake sediment and ice cores are widely accepted for climate reconstruction. Among other materials, these records are strongly influenced by the isotope value of precipitation as they developed (e.g., Jones, 2009; McCarroll and Loader, 2004; Lachniet, 2009; Sachse et al., 2012). A better understanding of isotopic variability in precipitation can enable better reconstruction of past environments. It has been widely known that the annual mean isotope value demonstrates strong correlation in space and time with temperature in high latitude regions (e.g., Dansgaard, 1964; Jouzel et al., 1997) and with precipitation amounts in lower latitude regions (e.g., Dansgaard, 1964; Rozanski et al., 1993). These empirically derived isotope/climate relationships have been widely used for the interpretation of the isotope proxy record in paleoclimate studies (e.g., White et al., 1997; Wang et al., 2001). However, the isotopic composition of precipitation is affected by a variety of factors such as water vapor source, trajectory of the water vapor transport, rainout history during the transport and local convective processes including post-condensational exchange processes (e.g., Araguás-Araguás et al., 2000). The multiple competing influences on isotope values have to be considered for better interpretation of isotope records (e.g., Fricke and O'Neil, 1999; Vachon et al., 2007; Sturm et al., 2010). In the tropics, various observational and modeling studies have been carried out to provide a greater depth of the interpretation of natural isotopic variability, leading to a common conclusion that isotopic variation in tropical precipitation is related to the large-scale convective activity associated with intraseasonal variation, rather than precipitation amount (e.g., Lawrence et al., 2004; Risi et al., 2008; Vimeux et al., 2011; Kurita et al., 2011; Tremoy et al., 2012; Moerman et al., 2013). Since enhanced downdraft/subsidence associated with a convective system transports moisture with low isotopic ratio to the boundary layer, the more intense the convection, the stronger the downdraft and subsidence and the more depleted the isotopic composition in the boundary layer vapor feeding the

CPD
10, 3989–4032, 2014

convective system (vapor recycling) will be. In a convectively active region/period, convective rainfall is sustained for several days and the successive rainfall increases the precipitation over a region and decreases the isotopic values of precipitation with an increase in the contribution of recycled vapor (Kurita, 2013). This interpretation proposes that isotope records from the tropical region can be used to reconstruct past large-scale convective activity.

For mid-latitude regions, the number of studies using event or daily-based isotope data are rapidly increasing in an effort to identify climate drivers controlling isotopic variability on seasonal to annual time scale. For example, in the United States, inter-event isotopic variation in response to changes in storm track have been reported (Lawrence et al., 1982; Friedman, 2002; Burnett et al., 2004). Recently, **?** showed that changes in vapor sources are manifest in the isotopic composition of precipitation that falls along the western coast of the US. The most isotopically enriched values occur over California when storms supply subtropical marine air with relatively enriched isotopic values from the Pacific. In contrast, storms bringing moisture from the northern Gulf of Alaska are related to the most depleted events. The same feature has been reported with Irish (Dublin) precipitation in northwestern Europe (Baldini et al., 2010). On the other hand, results of observation in southern Australia revealed the close relationship of isotopes in precipitation to the prevailing synoptic scale weather pattern (Treble et al., 2005; Barras and Simmonds, 2008, 2009; Crawford et al., 2013). Treble et al. (2005) found that large amounts of precipitation with lower isotope values occurred when well-developed large-scale low-pressure systems passed close to the observation site in Tasmania. By contrast, when the center of these storms passed much further south of Tasmania, weak rainfalls were isotopically enriched. In addition, Crawford et al. (2013) highlighted the role of cumulative rainfall amounts (rainout history) during the transport of moisture before reaching the observation site to the inter-storm variability in Australian precipitation isotopes. These results demonstrate that isotopic variability in individual local precipitation is closely related to the synoptic scale meteorological conditions.

CPD
10, 3989–4032, 2014

In contrast from the tropics, historical monthly-based isotope records of precipitation are available for the mid-latitude regions. More than 50 years of long-term data of precipitation isotopes from around the world is archived in the Global Network of Isotopes in Precipitation (GNIP), coordinated by the International Atomic Energy Agency (IAEA) in cooperation with the World Meteorological Organization (WMO) (e.g., IAEA-WMO, 2013). This network is uniquely dense mid-latitude over the Northern Hemisphere, allowing for detailed analyses of controls on inter-annual variability of isotopes in mid-latitude precipitation. Recent studies showed that inter-annual isotopic variability in European winter precipitation is related to the North Atlantic Oscillation (NAO) index (Baldini et al., 2008) and hemisphere-wide teleconnections associated with the Arctic Oscillation (AO) (Field, 2010). Birks and Edwards (2009) found a strong Pacific-North American (PNA) control on isotopic composition of Canadian winter precipitation. These new findings demonstrate that the variability in the isotopic composition of seasonal precipitation occur in response to changes in the pattern of large-scale atmospheric circulation. Therefore, coupled with the findings from the event-based record of precipitation isotopes, we can say that isotopic variation in mid-latitude precipitation is not directly controlled by temperature and precipitation amounts but that it mostly depends on large-scale atmospheric circulation. Proving the last statement in order to provide a seamless explanation of isotopic variability in association with atmospheric circulation at multiple temporal scales (inter-annual, seasonal, and event scales) will require clearly showing that changes in short-term isotopic variability affect inter-annual isotropic variations.

The central purpose of this study is to improve our knowledge of how climate changes affect isotopic content in precipitation. In this study, using new one-year long event-based isotope values in precipitation and long-term records of monthly precipitation isotopes in central Japan, we sought to unveil the mechanism that exerts large-scale atmospheric circulation controls on isotopic compositions in precipitation at multiple time scales from event- to inter-annual scales. Japan is a preferable location for studying atmospheric circulation controls on isotopic values because it is in the East

CPD
10, 3989–4032, 2014

Asian monsoon region (Yihui and Chan, 2005) and most of the moisture-formed precipitation originates from the ocean (Yoshimura et al., 2004). We can therefore ignore secondary influences such as mixing with continental-recycled moisture and over-land rainout. Historical 17 years record of oxygen and hydrogen isotopic composition of precipitation at the Tokyo station is archived in the GNIP dataset. The 17 year long Tokyo station record in GNIP provides enough length for a discussion of the physical structure of the inter-annual isotopic variability in response to changes in atmospheric circulation. First, we identified key atmospheric processes controlling the storm-to-storm isotopic variations through an analysis of back trajectories and classification of precipitation systems. Then we applied the identified processes to explain inter-annual variability and examine whether factors controlling event-scale isotopic variability can account for more long-term isotopic variability. Finally, we propose a new interpretation of the isotope proxy records in Japan and the surrounding region.

2 Data and methods

2.1 Climate summary at observation site

The isotope observation was conducted at Nagoya (35.15° N 136.97° E, 50 m a.s.l.) located on the Pacific side of the central Japan (Fig. 1). The mean annual rainfall at Nagoya is about 1500 mm, falling almost entirely as rain. The precipitation in summer is much higher than that in winter. GNIP Tokyo station is also located on the Pacific side. The climate in Japan has clear seasonal differences due to the influence of the seasonal monsoon wind. Japan is spread across the northeastern edge of the East Asian Monsoon (EAM) region, and the EAM has distinct warm summer and cold winter monsoons. The winter monsoon is a cold and dry monsoon in which northwesterly winds are dominant (Fig. 2a). In winter, the Siberian anticyclone (also called Siberian High) sits over the eastern Siberia with a strong Aleutian low pressure to its east, pushing away the accumulated cold from Siberia with north-westerlies along the eastern flank

CPD
10, 3989–4032, 2014

of the Siberian High (e.g., Joung and Hitchman, 1982). The subsequent cold and dry airflow into the relatively warmer ocean triggers enhanced evaporation and convective activity over the Japan Sea (e.g., Manabe, 1957; Ninomiya, 1968). Therefore, winters are snowy all along the Japan Sea coast. In contrast, the weather is sunny and bright along the Pacific side because most of the snow falls out as the air mass traverses the mountain range that runs centrally along Japan. On the Pacific side, winter precipitation is usually brought by cyclones advecting off the south coast of Japan (called Nangan cyclones) and associated fronts embedded in the cyclone passing through the Japan Sea (called Japan Sea cyclone) (Chen et al., 1991; Kusaka and Kitahara, 2009; Adachi and Kimura, 2007) (see Fig. 1).

In comparison during the summer, low-level winds reverse primarily from northwesterlies to southerlies (Fig. 2b). The summer monsoon season is characterized by two active rainfall periods separated by a break phase (see Yihui and Chan, 2005; Ninomiya and Murakami, 1987, for a detailed review). The first rainy period is the northward-migrating rainband known as Baiu in Japan. This Baiu rainband forms on the boundary between the maritime tropical air mass and both continental and maritime polar air masses, and is maintained by moisture supplied by southerlies from the subtropics. The Baiu rainband appears in mid-May in the southernmost regions of Japan, and then migrates slowly northward across Japan from early June to mid-July. In mid-July, the Baiu rainband rapidly jumps to northern China and Korea, ending the first rainy period. After some period, the Baiu, which had moved northward in early summer, retreats southward to begin the second rainy period that runs from the end of August to early October (called Akisame in Japan). At the Pacific side in central Japan, the second rainy period is not so obvious compared with the first period. In addition to the Baiu and Akisame rainfall, typhoons occasionally bring large amounts of rainfall to Japan in the summer season. The number of typhoons approaching the Japanese archipelago is much higher in boreal and late summer than in the first rainy period.

CPD
10, 3989–4032, 2014

2.2 Isotope observation

A one-year long event-based precipitation sampling and continuous measurement of water isotopes was conducted at the campus of Nagoya University from June 2013 to June 2014. Throughout this paper, the isotopic concentrations are expressed in δ notation: δD or $\delta^{18}O = (\frac{R_{sample}}{R_{V\text{-}SMOW}} - 1) \times 1000$, where R is the isotopic ratio (HDO/H_2O or $H_2^{18}O/H_2^{16}O$). V-SMOW is Vienna Standard Mean Ocean Water.

Precipitation samples were collected in a capped HDPE bottle with a plastic funnel when precipitation was not observed in the previous few hours or at 8 a.m. LT if precipitation had ended at midnight. To prevent post-evaporation from the collected samples, stable isotope analysis was performed as soon as possible after the collection using cavity ring-down spectroscopy isotopic water analysis (model L1102-i; Picarro Inc., Sunnyvale, CA, USA) with a CTC Analytics autosampler (model HTC-PAL; Leap Technologies, Carrboro, NC, USA). Measurement precision, including internal and external variations, was better than ±0.2‰ for $\delta^{18}O$ and ±2.0‰ for δD. Analytical uncertainty in d-excess for our measurements was better than 2.1‰.

Water vapor isotope was measured using both a WVIA (model DLT-100) manufactured by Los Gatos Research Inc. (LGR Inc., Mountain View, CA, USA) and a conventional cold trap method, which was used in Kurita et al. (2013). Outdoor air (15 m above the ground) was drawn to the WVIA and the cold trap system with a 5 m length of Teflon tubing via the external pump at a flow rate of 1.5 L min^{-1}. As for laser-based measurement, δD and $\delta^{18}O$ in the ambient air were recorded by the WVIA at 1 Hz. On the other hand, water vapor samples were collected in the trap at 8 a.m. LT every day and were analyzed by the same method for the precipitation samples. Data calibration for laser-based measurement followed the procedure developed by Kurita et al. (2012), without the correction for time-dependent isotope drift. For δD measurements, the instrumental drift was less than the analytical error related to the cold trap method, although the instrumental drift in $\delta^{18}O$ values cannot be deemed negligible compared with the results obtained from the cold-trapped approach. Here, therefore, we focus on δD data.

CPD
10, 3989–4032, 2014

The H_2O concentration-δD response was evaluated by humidity bias defined as the δD difference of water vapor between WVIA data and cold trap samples at each H_2O concentration. We calculated a second order polynomial fitting curve using one-year long humidity bias data, and then applied it for calibrating the H_2O-concentration dependence. To evaluate the validity of WVIA-measured δD values, the corrected WVIA data was compared to the results obtained from the cold trap approach. We calculated the time-averaged WVIA-measured δD values during vapor trapping and then compared them with the cold trap values for the same sampling periods. The day-to-day variation of the δD from cold trap samples matched the WVIA values as expected, although the short-term variation (within a day) could not be resolved by the measurement using the trapping approach. The mean value of the deviations of 298 samples was 0.4 ± 2.8‰. This value is worse than the analytical error associated with the cold trap method (±2.0‰), but is acceptably smaller than the natural variability. The optimum average time of the WVIA was examined using the Allan variance method (Werle et al., 1993) by Sturm and Knohl (2010) who concluded that the highest precision was obtained from a 10- to 15 min average. We therefore used 10 min-average data for the analysis.

The long-term records of the oxygen isotopic composition of precipitation ($\delta^{18}O$) at the Tokyo station (35.7° N 139.8° E, 4 m a.s.l.) archived in the GNIP database were used to examine the inter-annual seasonal isotopic variation. The data consist of monthly precipitation samples and are available from 1962 to 1979. The variation in oxygen isotopic content of precipitation mirrors that of the hydrogen isotopic content.

2.3 Meteorological data

Surface meteorological data was obtained from the local meteorological observatory located nearest each isotope monitoring station (Nagoya University and GNIP Tokyo station). Hourly meteorological variables such as barometric pressure, relative humidity, air temperature, wind speed, wind direction, incoming solar radiation, and precipitation amounts are available from the Japan Meteorological Agency (JMA)

CPD
10, 3989–4032, 2014

(http://www.data.jma.go.jp/gmd/risk/obsdl). As for large-scale precipitation field data, radar precipitation data calibrated with rain gauge observations (Radar-AMeDAS precipitation data) provided by JMA was used in this study. Radar-AMeDAS is 10 min data that entirely covers all the Japanese islands and the surrounding oceans. The horizontal resolution of this data is 5 km. Data is available from 1988. The Japanese 55 year reanalysis project (JRA-55) dataset (Ebita et al., 2011) were used to examine synoptic scale weather condition. The JRA-55 data are on a horizontal 1.25° × 1.25° grid with 37 vertical layers from 1000 to 1 hPa.

2.4 Back trajectory analysis

To estimate cumulative precipitation during the transport along the air mass pathway, backward air mass trajectories were calculated for each precipitation event using the Hybrid Single-Particle Lagrangian Integrated Trajectory (HYSPLIT) Model (Version 4.0) provided by the National Oceanographic and Atmospheric Administration Air Resources Laboratory (NOAA ARL) (Draxler and Rolph, 2003). Wind fields provided by NCEP (National Center for Environmental Prediction) Global data assimilation system (GDAS), which is a 1.0° × 1.0° horizontal grid, were used as forcing data. Trajectories were calculated from several different points around the observation site (0.5° × 0.5°) at hourly intervals while rainfall was recorded at the site. Each 30 min position along the 24 h back trajectories was archived. The cumulative rainfall (P_{cumul}) was calculated as the sum of precipitation along the trajectories before arriving at the site. In order to obtain the time average value during each event, the calculated cumulative precipitation was weighted by the observed hourly precipitation amount at the measurement site:

$$P_{\mathrm{cumul}} = \frac{\sum_{t=0}^{m} R_t \left(\sum_{i=0}^{n} P_i / n\right)}{\sum_{t=0}^{m} R_t} \quad (1)$$

where the subscript m indicates total rainfall hours and n represents the number of trajectories at each hour, P_i is the cumulative rainfall for each trajectory, and R_t is the

CPD
10, 3989–4032, 2014

recorded rainfall amount at the site. In Japan, precipitation mostly originates from the surrounding oceans (Yoshimura et al., 2004). We can therefore assume that cumulative rainfall from the source region to the site can be identical with the total rainfall amount passing through a precipitating system that provides rainfall at the observation site. Because trajectories do not travel far away from Japan, the major source of uncertainty for cumulative rainfall is related to the quality of the precipitation field data, rather than the trajectory uncertainty. Here, we used 30 min averaged Radar-AMeDAS data, which was re-gridded to a 0.5° resolution to estimate precipitation amount at each trajectory position.

2.5 Precipitation classification

In the summer monsoon season, a quasi-stationary rainband appears at the boundary between warm air and relatively cold air and is characterized by a large gradient of equivalent potential temperature θ_e (Ninomiya, 1984) (see Fig. 2b). At the center of this rainband, θ_e in the lower atmosphere is around 335 K and θ_e gradually decreases (increases) toward the north (south) (Tomita et al., 2011; Kanada et al., 2012). In this study, we calculated the vertically averaged (925–850 hPa) equivalent potential temperature $\langle\theta_e\rangle$ around the observation site, and then the summer precipitation was divided into warm and cold events depending on the $\langle\theta_e\rangle$ of the air mass-induced precipitation. The warm rainfall event produced by (sub)tropical maritime air mass was defined as (1) those that $\langle\theta_e\rangle$ exceed 335 K around the observation site or (2) the southerlies from the subtropics regions ($\langle\theta_e\rangle > 335$ K) that transport moisture to feed rain-bearing systems over the observation site. On the other hand, cold rainfall events were defined as residual cases, or those that did not satisfy both conditions.

In the winter monsoon season, the precipitation events were classified into three types of cyclonic precipitation and into others (O-type). The surface cyclones were identified using the 6 hourly Sea Level Pressure (SLP) field in the JRA-55 dataset, and the cyclonic precipitation events were classified depending on the route for cyclones as follows: Japan Sea cyclone (J-type), Nangan cyclone (N-type), and intermediate

CPD
10, 3989–4032, 2014

cyclone type (I-type). The Japan Sea cyclone type corresponds to the rainfall from the frontal system related to the Japan Sea cyclone. The Nangan cyclone type is a cold rainfall or snowfall event that occurs at the north of the surface warm front moving eastward along the southern coast of Japan. Intermediate type cyclones travel over the main island of Japan, with the center of the cyclones passing near the study site. Although most precipitation events are derived by extratropical cyclone connected with fronts, occasionally small-scale convective clouds traveled from the Japan Sea coast, bringing weak snowfall or rainfall to the site (O-type).

3 Results

3.1 Seasonal cycle

One-year records of δD in both water vapor and precipitation are shown in Fig. 3, together with temporal variation in meteorological variables. Continuous δD variation in surface vapor shows that the seasonal cycle is weak, and that sub-monthly or intra-seasonal variation is more dominant. On the other hand, meteorological variables (surface air temperature, water vapor concentration, and precipitation amounts) exhibited distinct seasonality with the maximum value in summer and the minimum in winter. Additionally, clear seasonality of the d-excess, with higher values in winter and lower values in summer, was seen in Fig. 3b. This reflects the change in moisture source by the reversal of the monsoon wind direction. In winter, northerly winds push cold and dry continental air across the warmer water over the Japan Sea, with subsequent evaporation occurring under conditions with a large humidity deficit and a strong temperature contrast between the surface air temperature and the sea surface temperature. As noted previously by numerous studies (e.g., Gat et al., 2003; Uemura et al., 2008), this leads to relatively high d-excess in surface water vapor. In contrast, southerly winds transport warm maritime air with relatively low d-excess to Japan in the summer (Kurita, 2013). Unclear seasonality of δD in surface vapor means that changes in moisture

CPD
10, 3989–4032, 2014

source from the Pacific to the Japan Sea does not affect the δD values for the most part. However, δD in surface vapor was sensitive to precipitation events. δD decreases appeared mostly in association with the rainfall events and the amplitude of the depletion was closely related with the δD values in precipitation. As shown in Fig. 3a, the calculated δD of vapor in isotopic equilibrium with precipitation agreed with the observed values in surface vapor. The temporal isotopic variability of surface vapor during a year can therefore be identical to the variation in precipitation. This time-series data highlights the control by short-term isotopic variability on seasonal or more long-term mean isotopic values. This time scale matches well with the synoptic disturbance activity.

The distribution of δD in individual precipitation events is shown in Fig. 4a. Interestingly, the precipitation-weighted annual mean δD value (−56 ‰) does not correspond to the dominant bin of δD value, and is significantly lower than the arithmetic mean (−40 ‰). The winter (DJFM) and summer (JJAS) mean values are also lower than the arithmetic mean annual precipitation. The same features can be seen in δ^{18}O (Fig. 4b). These suggest that the precipitation events with lower δD values makes a larger contribution to the seasonal and annual mean values, and the variability of annual or seasonal mean δD value is attributable to the change in relative contribution of storm events. However, for all the precipitation events (n = 78), the negative correlation between δD in precipitation and precipitation amount (the amount effect) was weak (R^2 = 0.167), although samples with relatively the higher (lower) δD values were characterized by the low (high) rainfall events (see Fig. 4a). The storm-to-storm isotopic variation may be controlled by not only the local rainout, but also by upstream atmospheric conditions such as moisture sources and rainout history during the transport.

3.2 Summer precipitation

During the summer rainy season, sub-synoptic scale rain fronts forms between a warm air mass from subtropical maritime regions and a cold air mass from both continental and maritime polar regions (see Fig. 2b). In the first rainy season (Baiu), rainfall occurs in association with the north-south displacement of this front. Notably different equiv-

CPD
10, 3989–4032, 2014

alent potential temperatures (θ_e) characterize the cold and warm air masses. θ_e at the observation site varies considerably depending on the north-south displacement of this front. In addition, as shown in Fig. 5, the temporal variation of δD in surface vapor was associated with changes in vertical average of θ_e ($\langle\theta_e\rangle$). The highest δD peaks corresponded to southerly flows supplying warm maritime air to the site, while abrupt δD decreases appeared in association with a southward shift of cold air mass. On the other hand, rainfall events during the second rainy season (Akisame) are usually derived from the low-pressure systems connecting with fronts. Low-level southerly winds east of the cyclone transport warm air with high $\langle\theta_e\rangle$, while relatively cold air with low $\langle\theta_e\rangle$ is supplied by northerly winds. In Fig. 5, the short-term increases and decreases in $\langle\theta_e\rangle$ correspond to the passage of the frontal systems and troughs, and similarly to the first rainy season, δD in surface vapor relates well to the $\langle\theta_e\rangle$ variations. These features are identical with the results obtained from the observation in 2010 (Kurita et al., 2013). In addition, this temporal isotopic variation mirrors that of precipitation. Relatively high δD in precipitation matched the warm rainfall events, and lower δD was observed when cold air inflow occurred. These are classified as cold rainfall events. We concluded from this that the δD difference between warm- and cold-type rainfall reflects changes in air mass sources. On 24 August (labeled 1 in Fig. 5), δD in precipitation was relatively low, although $\langle\theta_e\rangle$ was similar to that in subtropical air (> 335 K). The weather map showed that southerly winds from the subtropics did not arrive at the observation site and the frontal system was displaced to the south of the observation site. The rainfall event therefore corresponds to cold rain and not warm rain.

We investigated the influence of rainout history from the upstream region. The relationship between the δD in individual precipitation events and cumulative rainfall along the trajectories (P_{cumul}) of over 9 h is displayed in Fig. 6a. Although δD of warm rainfall events are plotted above those from cold events, the gradual decreasing trend in δD with P_{cumul} is more clearly evident. The correlation coefficient gradually improved with increasing integration time and then reached the highest value ($R^2 = 0.654$) at 9 h (see inset in Fig. 6a). The sample labeled "A" in Fig. 6a (labeled "2" in Fig. 5)

CPD
10, 3989–4032, 2014

was ignored from the regression analysis because this sample was obtained from the downstream-propagating fully developed convective line, in which the influence of vapor recycling associated with mesoscale convective systems may significantly reduce rainfall δD (Kurita, 2013). The lowest δD was observed with the maximum P_{cumul} when the intense typhoon passed southeast of the site in the middle of October (labeled TY in Fig. 6a). An intense precipitation area extended from east and north of the center of the typhoon along the cyclonic flow with the site being located in the downstream area of the precipitation (the northwestern side of the typhoon). Also since northeasterly winds at the northern side of the typhoon transport low $\langle\theta_{\mathrm{e}}\rangle$ air from the north, the contribution of this air to the typhoon precipitation may act to further decrease δD. For summer precipitation, including October, good correlation between δD in precipitation and P_{cumul} indicates that cumulative precipitation while air mass passed through the rain-bearing systems is a major driver of the storm-to-storm variability in δD.

3.3 Winter precipitation

In winter, precipitation occurs in association with the passage of eastward-moving extratropical cyclones connected with fronts (see Fig. 1). We examined the isotopic variability arising from changes in moisture sources. According to the conveyor belt concept (Carlson, 1980), a winter cyclone consists of three major air streams: (a) the warm conveyor belt (WCB), (b) the cold conveyor belt (CCB) and (c) the dry intrusion. The WCB is a stream of relatively warm moist air and originates over the warm waters of Pacific. This air flows northward toward the center of the cyclone and supplies moisture to a warm frontal rainband. The CCB originates to the northeast of the cyclone, and easterly or northeasterly winds north of the cyclone transport this air westward, and feeds a cold frontal rainband. Therefore, the precipitation associated with the cold front mainly originates from the mid- or high-latitude regions.

In the case of the Japan Sea cyclones, the low pressure centers moved across the middle of Japan Sea. Figure 7 shows that warm air with high $\langle\theta_{\mathrm{e}}\rangle$ was injected into the high-latitude region across the observation site when this type of precipitation ap-

CPD
10, 3989–4032, 2014

peared. The fact that these warm air injections correspond to the highest peaks of δD in surface vapor indicates that the WCB supplies moisture northward with enriched δD. Two events of intermediate type (I-type) also showed similar features to the Japan Sea type (J-type). This indicates that the WCB reaches near the center of the cyclone. In contrast, the δD depletions occurred in association with the passage of the Nangan cyclones. The major route for the Nangan cyclone is off the south coast of Japan from the East China Sea. Unlike the Japan Sea cyclone, a cold frontal rainband fed by the CCB was primarily responsible for precipitation along the Pacific coast of East Japan (Takano, 2002). The CCB transports moisture originating from mid- and high-latitude regions, and as shown by Kurita (2013), the isotopic content of marine surface vapor decreases toward the high latitude regions. Therefore precipitation in association with the Nangan cyclone (N-type) is characterized by relatively lower δD values than the others. We further, examined the influence of rainout history along the trajectories as an additional source of the δD variability in winter. Excepting N-type events, a robust trend of lower δD with increasing P_{cumul} was evident in Fig. 6b. However, δD in N-type precipitation were distributed without a clear trend in relation to P_{cumul} and were plotted below the regression line obtained from both J-type and I-type samples. Two N-type events observed in March (plotted near the regression line) were considered to be I-type rather than N-type because warm air with high $\langle\theta_{\mathrm{e}}\rangle$ was transported beyond the center of the cyclone and reached near the observation site (Fig. 7). These results indicate that the progressive depletion of δD in vapor-produced rainfall along the pathway from the moisture source region is not a major contributor to large δD depletion in N-type precipitation. Distinctive changes in the isotopic composition of moisture that feeds precipitation systems is likely a more important factor influencing the large isotopic variability in winter.

CPD
10, 3989–4032, 2014

4 Inter-annual isotopic variation

An event-based record of δD in precipitation coupled with a continuous record of δD in surface water vapor elucidates the primary drivers of storm-to-storm isotopic variations for the central Japan. However, this result is only based on data for one year, so that further investigation is necessary to confirm the control on inter-annual variability in precipitation isotopes. Here, using the historical 17 year record of isotopes in precipitation from the GNIP Tokyo station, we examined whether the identified key drivers can account for the inter-annual isotopic variations. In this study we used oxygen isotopes δ^{18}O as a substitute for δD, because the oxygen isotope record of precipitation in Tokyo has been recorded much longer than for δD. The δ^{18}O variation of precipitation mirrors that of hydrogen isotopic content.

In summer, δD (δ^{18}O) in individual rainfall event varied widely from event to event, ranging from close to 0 ‰ (0 ‰ for δ^{18}O) to less than −100 ‰ (−13 ‰), and the wide range of isotopic variability was mainly attributed to the cumulative rainfall along the trajectories (Fig. 6a). The isotopic minima in the summer precipitation corresponded to the maxima of cumulative rainfall while air mass the travels through the precipitating systems. To investigate whether this effect was sufficient to explain the inter-annual isotopic variability, the relationship between isotopic content in precipitation and regional average precipitation amounts was examined. Because the observation period for when monthly precipitation was collected in the GNIP Tokyo station (1962–1979) is prior to the Radar-AMeDAS data, we could not calculate cumulative rainfall amounts in the same way as mentioned above. The inset in Fig. 6a shows gradual improvement of the correlation coefficient with increasing integration time. However, the largest improvement was observed when the local precipitation amount was replaced with the area-averaged precipitation amount. A small correlation coefficient ($R^2 = 0.0071$, p value = 0.63) between δD and the local precipitation amount was improved up to $R^2 = 0.475$ (p value < 0.0001) between δD and the area-averaged precipitation amount (the value at $t = 0$ in the inset in Fig. 6a). This demonstrates that we can use area-

CPD
10, 3989–4032, 2014

averaged rainfall amounts as a substitute for cumulative rainfall amounts during air mass travel in the precipitating system. In this study, Global Precipitation Climatology Center monthly precipitation (GPCC) dataset version 6 (Schnider et al., 2011) was used to obtain area-averaged precipitation. The relationship between δ^{18}O and area-averaged precipitation amount for the summer precipitation from 1962 to 1979 is plotted in Fig. 8. All data was weighted by monthly precipitation to calculate the summer average and expressed as normalized anomalies (see details in figure caption). Inter-annual variability in monthly rainfall δ^{18}O was completely independent from the precipitation amount. In addition, δ^{18}O in the summer averaged precipitation showed no significant isotopic depletion with precipitation amount. Different from the storm-to-storm isotopic variability, rainout history does not have a significant influence on the inter-annual variability in the summer rainfall δ^{18}O. Next, we explored the influence of moisture source on the inter-annual isotopic variation. In summer, southerly flows transport moisture with relatively higher δ^{18}O, with the warm rainfall type being relatively enriched in heavy isotopes compared with the other rainfall events (Fig. 5). The increase in the contribution of warm rainfall to the total summer precipitation must lead to richer isotopic values in summer average precipitation. Here, we divided daily precipitation into warm and cold events using the $\langle\theta_e\rangle$ field, and then calculated the cumulative warm rainfall amounts for the summer. To examine how changes in contribution of warm rainfall were manifested in the isotopic values in summer precipitation, we defined the warm rain ratio (R_{WR}) as the ratio of cumulative warm rainfall to the total summer precipitation. During the period of 1962–1979, the R_{WR} changes widely year by year, ranging from 0.35 to 0.85 and the inter-annual variation in δ^{18}O in summer precipitation matches well with R_{WR} (Fig. 9a). The correlation between δ^{18}O and R_{WR} for each individual month was as follows: June (R^2 = 0.630), July (R^2 = 0.719), August (R^2 = 0.413), and September (R^2 = 0.389). This indicates that year-to-year variations in R_{WR} particularly influence the inter-annual variability in rainfall δ^{18}O during the first rainy season (June–July). With more than half of summer precipitation occurring during the first rainy season, a high correlation coefficient (R^2 = 0.627, p = 0.0001) was

CPD
10, 3989–4032, 2014

observed for the precipitation-weighted summer average (Fig. 10a). From this we can conclude that variations in the southerly moisture flux are the primary driver of inter-annual variations in the summer precipitation $\delta^{18}O$.

Winter precipitation was usually related to extratropical cyclones, and inter-event isotopic variability was linked to their storm tracks. Southerly storms classified as Nangan-type induce cold precipitation with the most depleted isotope values, as northerly winds bring cold and humid air with lower isotopic values to the observation site. Clearly, the greater the contribution by Nangan-type precipitation to the total winter precipitation, the more depleted the isotopic content in winter average precipitation will be. Using the SLP field, we identified the date when Nangan cyclones passed through the site, and then calculated cumulative daily precipitation produced by Nangan cyclones during winter season. As expected, year-to-year variation in the precipitation-weighted $\delta^{18}O$ in winter precipitation negatively correlated with the relative contribution of Nangan-type precipitation to total winter precipitation ($R_{\text{N-type}}$) in Fig. 9b. The positive (negative) peaks of $R_{\text{N-type}}$ (1965, 1969, 1973 for positive; 1976 for negative) matched the relatively depleted (enriched) $\delta^{18}O$ in winter precipitation. Moreover, an abrupt increase of $\delta^{18}O$ in the mid-1970s occurred concurrently with a clear decreasing trend of $R_{\text{N-type}}$. Therefore, a statistically robust negative correlation ($R^2 = 0.483$, $p = 0.002$) was observed during the 1962–1979 period (Fig. 10b). From these, we can conclude that frequency and intensity of the Nangan cyclones have a significant impact on both individual precipitation and the winter averaged precipitation $\delta^{18}O$.

5 Discussion

The goal of this study is to understand the main driver controlling isotopic variability in precipitation at multi scales to provide a greater depth of interpretation on isotope based proxy. The historical 17 year record of isotopes in precipitation demonstrated that isotopic variability on an inter-annual time scale is primarily attributed to differences in

CPD
10, 3989–4032, 2014

the isotopic composition of the moisture source. An increased contribution of low (mid- or high) latitude moisture to precipitation acts to enrich (decrease) the precipitation isotopes. As discussed in previous studies (Baldini et al., 2008; Birks and Edwards, 2009; Field, 2010), inter-annual isotopic variation in Japanese precipitation could be linked to the large-scale atmospheric circulation change in response to natural climate variability. To investigate circulation features influencing inter-annual isotopic variability in precipitation, correlation maps were constructed between monthly anomalies of the $\delta^{18}O$ at Tokyo and sea level pressure (SLP) fields. During summer, there is significant negative correlation over the Japan Sea (Fig. 11a). The western North Pacific subtropical high (WNPSH) is more stable and expands to higher latitudes across the Japanese archipelago from early June to mid-July. Negative SLP anomalies therefore indicate that subtropical high pressure is weak and does not extend to this region in mid summer. Since isotopically enriched air was transported by south-westerlies on the northwestern edge of the WNPSH (Fig. 2b), weak high pressure may result in lower $\delta^{18}O$ of summer precipitation. To verify this explanation, we constructed composite maps of $\langle\theta_e\rangle$ corresponding to the years that the isotopic content of summer precipitation is significantly lower than the climate average (1963, 1966 and 1970), as shown in Fig. 12. The distinct negative $\langle\theta_e\rangle$ anomaly over the Japan Sea in July closely matched the negative correlation of SLP field. In July, anomalous northerlies in association with the passages of low pressure systems are dominant in the negative $\langle\theta_e\rangle$ anomaly region, and the $\langle\theta_e\rangle$ anomaly gradually increased to the southward. It was interpreted that the northward extension of the high-pressure system was blocked by cold airflow from the high-latitude region. The negative $\langle\theta_e\rangle$ anomaly at Tokyo indicates that the contribution of southerly moisture in summer precipitation becomes lower than for a normal year. In Fig. 11a, we can also see the teleconnected signature over the western tropical Pacific region, which suggests that enhanced (weakened) convective activity over this region results in enriched isotopic composition in summer precipitation at Tokyo. This matches a teleconnection called the Pacific-Japan (PJ) pattern, a meridional dipole of sea level pressure variability (Nitta, 1987; Kosaka and Nakamura, 2006). A positive PJ

CPD
10, 3989–4032, 2014

pattern is related to negative SLP anomalies, corresponding to enhanced convection over the tropical western Pacific and anomalous intensification of the WNPSH. Enhanced convective activity to the east of the Philippines therefore leads to a stronger southerly flow to Japan and subsequently to the relatively enriched isotopic content of summer precipitation. It is well known that there are negative correlations between the PJ pattern and preceding wintertime El Niño/Southern Oscillation (ENSO) (e.g. Wang and Zhang, 2002). The expectation was for a correlation between δ^{18}O variability and ENSO through the PJ pattern. However there is no significant correlation between them. The reason is believed to be that the study period (1962–1979) is prior to the ENSO regime shift in which El Niño's influence on the subtropical northwestern Pacific becomes more influential after the mid-1970s climate regime shift (Xie et al., 2010). Figure 13 illustrates the atmospheric circulation in the case of intensification and weaking of the WNPSH.

For winter, an abrupt transition of both δ^{18}O and $R_{\text{N-type}}$ was observed during the mid-1970s (Fig. 9b). The timing of this transition matches the well-known the climate regime shift that took place in the North Pacific Ocean during the winter of 1976–1977 (e.g., Nitta and Yamada, 1989; Trenberth, 1990; Graham, 1994). This climate shift is characterized as a deepening of the Aleutian low since 1977, resulting in a more vigorous winter circulation over the northern Pacific. To remove the influence of this regime shift, we constructed a correlation map using winter data from 1962–1975 (Fig. 11b). Interestingly, the correlation map showed a similar teleconnection pattern to the well-known Arctic oscillation (AO) (e.g. Thompson and Wallace, 1998, 2000). The teleconnection signatures are characterized by a meridional dipole structure similar to the North Atlantic Oscillation (NAO) with a significant correlation over the north Pacific region. The winter precipitation δ^{18}O is negatively correlated with the winter AO index between 1962–1975 ($R^2 = 0.483$, $p = 0.002$). Particularly in the case of the negative AO winter, δ^{18}O are clearly heavier than those during the positive AO. This indicates that the Nangan cyclones during the negative AO tend to bring less precipitation to the observation site than during the AO positive. Nangan cyclone genesis usually oc-

CPD
10, 3989–4032, 2014

curs in the southeast China to the south of western Japan where cold airflow from the Siberian high (cold surge) meets warm subtropical air advected by southerly winds, and then moves eastward along the south coast of Japan (Saito, 1977; Chen et al., 1991; Takano, 2002; Adachi and Kimura, 2007). Meanwhile, the winter AO directly influences the cold surges over the east Asia through the changes in mid- and high-latitude circulation (e.g., Wu and Wang, 2002). During negative AO, both the Siberian high and the Aleutian low tend to be stronger than normal, and the atmospheric circulation becomes a favorable condition for cold surge occurrence related to southward expansion of the Siberian high (e.g., Jeong and Ho, 2005). Additionally, Park et al. (2011) noted that the cold surges during negative AO are stronger and longer lasting than those during the positive AO. These suggest that the transition zone between cold air from subarctic regions and warm air mass from the subtropics shift southward during the negative AO winter. Nangan cyclone genesis certainly may occur further south and their tracks may also shift southward, resulting in less precipitation amounts induced by this type of cyclones at Tokyo. Atmospheric circulation changes in response to the negative and positive AO, corresponding to the intense and weak East Asia Winter Monsoon (EAWM), is summarized in Fig. 13. It is noteworthy that the deepening of the eastward moving upper level trough and strengthening of the jet stream occurs during the negative phase of AO (Jeong and Ho, 2005). They contribute to enhance storm activity such as Japan Sea cyclones. Inter-annual variation in total winter precipitation is therefore less sensitive to the variability of precipitation induced by the Nangan cyclone. This interpretation can also explain the positive correlation with the Siberian high (Fig. 11b), which is not a typical AO pattern. The cold surges are related to northwesterlies along the east flank of the Siberian high, so that an intensified high-pressure system results in stronger cold surges that correspond to a negative AO. Furthermore, the abrupt decrease of $R_{\text{N-type}}$ across the 1976/77 climate transition is also consistent with the variation of the cold surge influenced by AO because an intensification of the Aleutian low corresponds to a larger meridional pressure gradient between the Aleutian low and Siberian high over the North Pacific. The cold surge after the transition

CPD
10, 3989–4032, 2014

should be stronger than before. From these indications, we can conclude that intensified EAWM considerably influences the genesis or the tracks of Nangan cyclones, and the variation in winter precipitation $\delta^{18}O$ is related to the various climate systems affecting the EAWM.

6 Conclusions

This study elucidates the primary driver of isotopic variability in Japanese precipitation at the multiple temporal scales: inter-annual, seasonal, and event-scales. An event-based one-year record of δD in precipitation at Nagoya in Japan showed less seasonal variations, but there is large variability in δD on a storm-to-storm basis. In summer, southerly flows transported moisture with relatively higher δD from subtropical marine regions, and the warm rainfall type was relatively enriched in heavy isotopes compared with the other rainfall events. In contrast, low δD were observed when northerly winds brought relatively cold air to the observation site. Some of the observed isotopic variability can be explained by changes in air mass sources, however this is not enough to have a large storm-to-storm isotopic range. The additional source of variability is attributed to rainfall amounts occurring both at the site and prior to the site. A clear decreasing trend in δD with cumulative rainfall over nine-hour back trajectories demonstrates that rainout history plays a dominant role on the storm-to-storm isotopic variability in the summer. The more isotopically depleted precipitation is from large-scale weather systems accompanied by prolonged rainfall over wide areas. In winter, low δD occurred when a cold frontal rainband associated with extra-tropical cyclones (Nangan cyclones) passed south of the Japan coast. Easterly or northeasterly winds north of the cyclone transport relatively cold air from the mid- or high-latitude regions to the site, and feed the cold frontal rainband. Therefore, the precipitation related to the Nangan cyclone is characterized by relatively lower isotopic values than those from another type of cyclone. It follows that the occurrence of Nangan cyclones is the most likely contributor to changes in winter mean precipitation δD.

CPD
10, 3989–4032, 2014

We explored if factors controlling storm-to-storm isotopic variability can account for inter-annual isotopic variability, using the historical 17 year record of isotopes in precipitation at the GNIP Tokyo station. The 17 year variation of summer precipitation $\delta^{18}O$ was independent of the variation in regional-scale summer precipitation, which is a substitute for cumulative rainfall along the trajectories. On the other hand, year-to-year variation of $\delta^{18}O$ related closely to changes in air mass sources. The relatively higher $\delta^{18}O$ in summer precipitation corresponded to the higher contribution of warm rainfall to the total summer precipitation, whereas the inter-annual variation of winter precipitation $\delta^{18}O$ correlated to the relative ratio of the rainfall from Nangan cyclones to the total winter precipitation. The frequent passage of intensified Nangan cyclones were responsible for increasing the contribution of cold frontal rainfall fed by northerly winds, and for further decreasing $\delta^{18}O$ in winter precipitation. These indicate that inter-annual isotopic variability in winter and summer precipitation in the central Japan is primarily related to changes in meridional moisture transport due to the distinctive difference in isotopic composition between low- and high-latitude moisture. During summer, the northward moisture transport into the central Japan is driven by the WNPSH. Inter-annual isotopic variation in summer precipitation corresponds to the strength of the WNPSH. Strong north-westerlies associated with the EAWM prevail over the East Asia during winter, and Nangan cyclone genesis or tracks are influenced by the intensity of the north-westerlies. Therefore, isotopic variability in winter can be linked to EAWM activity.

Progress in the understanding of isotopic variation of precipitation enables better reconstruction of past environments. With results obtained from other mid-latitude regions, it is no exaggeration to say that isotopic composition of mid-latitude precipitation is predominantly controlled by the large-scale atmospheric circulation, rather than precipitation amounts and temperature, and can therefore be used as a tool for the reconstruction of atmospheric circulation. Central Japan is replete with natural archives such as speleothems, tree ring cellulose, leaf wax, lake sediment, and proxy-reconstructed $\delta^{18}O$ or δD records allow us to examine the past activity of the WNPSH and the EAWM

CPD
10, 3989–4032, 2014

response to climate change extending back in time beyond the instrumental record. This long-term data must play an important role to distinguish between natural variability and anthropogenic-forced change in recent global climate change.

Acknowledgements. The authors gratefully acknowledge the NOAA Air Resources Laboratory (ARL) for the provision of the HYSPLIT transport and dispersion model and the relevant input files for generation of back trajectories. A Grant for Environmental Research Projects from the Sumitomo Foundation (Japan) supported this research. The Radar-AMeDAS data was acquired from the Research Institute for Sustainable Humanosphere (RISH), Kyoto University.

References

Adachi, S. and Kimura, F.: A 36 year climatology of surface cyclogenesis in east Asia using high-resolution reanalysis data, SOLA, 3, 113–116, 2007. 3995, 4010

Araguás-Araguás, L., Froehlich, K., and Rozanski, K.: Deuterium and oxygen-18 isotope composition of precipitation and atmospheric moisture, Hydrol. Process., 14, 1341–1355, 2000. 3991

Baldini, L. M., McDermott, F., Foley, A. M., and Baldini, J. U. L.: Spatial variability in the European winter precipitation δ^{18}O-NAO relationship: implications for reconstructing NAO-mode climate variability in the Holocene, Geophys. Res. Lett., 35, L04709, doi:10.1029/2007GL032027, 2008. 3993, 4008

Baldini, L. M., McDermott, F., Baldini, J. U. L., Fischer, M. J., and Möllhoff, M.: An investigating of the controls on Irish precipitation δ^{18}O values on monthly and event timescales, Clim. Dyn., 35, 977–993, 2010. 3992

Barras, V. J. I. and Simmonds, I.: Synoptic controls upon δ^{18}O in southern Tasmanian precipitation, Geophys. Res. Lett., 35, L02707, doi:10.1029/2007GL031835, 2008. 3992

Barras, V. and Simmonds, I.: Observation and modeling of stable water isotopes as diagnostics of rainfall dynamics over southeastern Australia, J. Geophys. Res., 114, D23308, doi:10.1029/2009JD012132, 2009. 3992

bibitem[Berkelhammer et al.(2012)Berkelhammer, Stott, Yoshimura, Johnson, and Shinha]Berkelhammer2012 Berkelhammer, M., Stott, L., Yoshimura, K., Johnson, K., and

CPD
10, 3989–4032, 2014

Shinha, A.: Synoptic and mesoscale controls on the isotopic composition of precipitation in the western United States, Clim. Dyn., 38, 433–454, 2012.
Birks, S. and Edwards, T.: Atmospheric circulation controls on precipitation isotope–climate relations in western Canada, Tellus B, 61, 566–576, 2009. 3993, 4008
Burnett, A. W., Mullins, H. T., and Patterson, W. P.: Relationship between atmospheric circulation and winter precipitation $\delta^{18}O$ in central New York State, Geophys. Res. Lett., 31, L22209, doi:10.1029/2004GL021089, 2004. 3992
Carlson, T.: Airflow through midlatitude cyclones and the comma cloud pattern, Mon. Weather Rev., 108, 1498–1509, 1980. 4003
Chen, S.-J., Kuo, Y.-H., Zhang, P.-Z., and Bai, Q.-F.: Synoptic climatology of cyclogenesis over east Asia, 1958–1987, Mon. Weather Rev., 119, 1407–1418, 1991. 3995, 4010
Crawford, J., Hughes, C. E., and Parkes, S. D.: Is the isotopic composition of event based precipitation driven by moisture source or synoptic scale weather in the Sydney Basin, Australia?, J. Hydrol., 507, 213–226, 2013. 3992
Dansgaard, W.: Stable isotopes in precipitation, Tellus, 16, 436–468, 1964. 3991
Draxler, R. and Rolph, G.: Hybrid Singlee-Particle Lagrangian Integrated Trajectory (HYSPLIT), Model released from NOAA ARL READY NOAA Air Resources Laboratory, Silver Spring, MD., http://ready.arl.noaa.gov/HYSPLIT.php, last access: 30 April,2014, 2003. 3998
Ebita, A., Kobayashi, S., Ota, Y., Moriya, M., Kumabe, M. R., Onogi, K., Harada, Y., Yasui, S., Miyaoka, K., Takahashi, K., Kamahori, H., Kobayashi, C., Endo, H., Soma, M., Oikawa, Y., and Ishimizu, T.: The Japanese 55 year reanalysis JRA-55: an interim report, SOLA, 7, 149–152, doi:10.2151/sola.2011-038, 2011. 3998
Enomoto, T.: Interannual variability of the Bonin high associated with the propagation of Rossby waves along the Asian jet, J. Meteorol. Soc. Jpn., 82, 1019–1034, 2003. 4032
Field, R. D.: Observed and modeled controls on precipitation $\delta^{18}O$ over Europe: from local temperature to the Northern Annular Mode, J. Geophys. Res., 115, D12101, doi:10.1029/2009JD013370, 2010. 3993, 4008
Fricke, H. C. and O'Neil, J. R.: The correlation between $^{18}O/^{16}O$ ratios of meteoric water and surface temperature: its use in investigating terrestrial climate change over geologic time, Earth Planet. Sc. Lett., 170, 181–196, 1999. 3991
Friedman, I.: Stable isotpe composition of waters in the Great Basin, United States 1. Air-mass trajectories, J. Geophys. Res., 107, 1–14, doi:10.1029/2001JD000565, 2002. 3992

CPD
10, 3989–4032, 2014

Gat, J. R., Klein, B., Kushnir, Y., Roether, W., Wernli, H., Yam, R., and Shemesh, A.: Isotope composition of air moisture over the Mediterranean Sea: and index of the air–sea interaction pattern, Tellus B, 55, 953–965, 2003. 4000

Graham, N.: Decadal-scale climate variability in the tropical and North Pacific during the 1970s and 1980s: observations and model results, Clim. Dynam., 10, 135–162, 1994. 4009

IAEA-WMO: Global Network of Isotopes in Precipitation, The GNIP database, http://www-naweb.iaea.org/napc/ih/IHS_resources_gnip.html, last access: 31 March,2013, 2013. 3993

Jeong, J.-H. and Ho, C.-H.: Changes in occurrence of cold surges over east Asia in association with Arctic oscillation, Geophys. Res. Lett., 32, L14704, 2005. 4010

Jones, P. D.: High-resolution paleoclimatology of the last millennium: a review of current status and future prospects, Holocene, 19, 3–49, doi:10.1177/0959683608098952, 2009. 3991

Joung, C. H. and Hitchman, M. H.: On the role of successive downstream development in East Asian polar air outbreaks, Mon. Wea. Rev., 110, 1224–1237, 1982. 3995

Jouzel, J., Alley, R. B., Cuffey, K. M., Dansgaard, W., Grootes, P., Hoffmann, G., Johnsen, S. J., Koster, R. D., Peel, D., and Shuman, C. A.: Validity of the temperature reconstruction from water isotopes in ice cores, J. Geophys. Res., 102, 26471–26487, 1997. 3991

Kanada, S., Nakano, M., and Kato, T.: Projections of future changes in precipitation and the vertical structure of the frontal zone during the Baiu season in the vicinity of Japan using a 5 km-mesh regional climate model, J. Meteorol. Soc. Jpn., 90A, 65–86, 2012. 3999

Kosaka, Y. and Nakamura, H.: Structure and dynamics of the summertime Pacific-Japan teleconnection pattern, Q. J. Roy. Meteorol. Soc., 132, 2009–2030, 2006. 4008, 4032

Kurita, N.: Water isotopic variability in response to mesoscale convective system over the tropical ocean, J. Geophys. Res., 118, 10376–10390, doi:10.1002/jgrd.50754, 2013. 3992, 4000, 4003, 4004

Kurita, N., Noone, D., Risi, C., Schmidt, G. A., Yamada, H., and Yoneyama, K.: Intraseasonal isotopic variation associated with the Madden-Julian Oscillation, J. Geophys. Res., 116, D24101, doi:10.1029/2010JD015209, 2011. 3991

Kurita, N., Newman, B. D., Araguas-Araguas, L. J., and Aggarwal, P.: Evaluation of continuous water vapor δD and δ^{18}O measurements by off-axis integrated cavity output spectroscopy, Atmos. Meas. Tech., 5, 2069–2080, doi:10.5194/amt-5-2069-2012, 2012. 3996

CPD
10, 3989–4032, 2014

Kurita, N., Fujiyoshi, Y., Wada, R., Nakayama, T., Matsumi, Y., Hiyama, T., and Muramoto, K.: Isotopic variations associated with north-south displacement of the Baiu Front, SOLA, 9, 187–190, doi:10.2151/sola.2013-042, 2013. 3996, 4002
Kusaka, H. and Kitahara, H.: Synoptic-scale climatology of cold frontal precipitation system during the passage over central Japan, SOLA, 5, 61–64, 2009. 3995
Lachniet, M. S.: Climatic and environmental controls on speleothem oxygen-isotope values, Quanternary Sci. Rev., 28, 412–432, 2009. 3991
Lawrence, J. R., Gedzelman, S. D., White, J. W. C., Smiley, D., and Lazov, P.: Storm trajectories in eastern US D/H isotopic composition of precipitation, Nature, 296, 638–640, 1982. 3992
Lawrence, J. R., Gedzelman, S. D., Dexheimer, D., Cho, H., Carrie, G. D., Gasparni, R., Anderson, C. R., Bowman, K. P., and Biggerstaff, M. I.: Stable isotopic composition of water vapor in the tropics, J. Geophys. Res., 109, D06115, doi:10.1029/2003JD004046, 2004. 3991
Manabe, S.: On the modification of airmass over the Japan Sea when the outburst of cold air predominates, J. Meteorol. Soc. Jpn., 35, 311–326, 1957. 3995
McCarroll, D. and Loader, N. J.: Stable isotopes in tree rings, Quaternary Sci. Rev., 23, 771–801, 2004. 3991
Moerman, J. W., Cobb, K. M., Adkins, J. F., Sodemann, H., Clark, B., and Tuen, A. A.: Diurnal to interannual rainfall δ^{18}O variations in northen Borneo driven by regional hydrology, Earth Planet. Sc. Lett., 369, 108–119, 2013. 3991
Ninomiya, K.: Heat and water budget over the Japan Sea and the Japan island in winter season, J. Meteorol. Soc. Jpn., 46, 343–372, 1968. 3995
Ninomiya, K.: Characteristics of Baiu front as a predominant subtropical front in the summer northen hemisphere, J. Meteorol. Soc. Jpn., 62, 880–894, 1984. 3999
Ninomiya, K. and Murakami, T.: The Early Summer Rainy Season (Baiu) Over Japan, Oxford University Press, 1987. 3995
Nitta, T.: Convective activities in the tropical western Pacific and their impact on the Northern Hemisphere summer circulation, J. Meteorol. Soc. Jpn., 65, 373–390, 1987. 4008, 4032
Nitta, T. and Yamada, S.: Recent warming of tropical sea surface temperature and its relationship to the Northern Hemisphere circulation, J. Meteorol. Soc. Jpn., 67, 375–383, 1989. 4009
Park, T.-W., Ho, C.-H., and Yang, S.: Relationship between the Arctic oscillation and cold surges over east Asia, J. Climate, 24, 68–83, 2011. 4010

CPD
10, 3989–4032, 2014

Risi, C., Bony, S., Vimeux, F., Descroix, L., Ibrahim, B., Lebreton, E., Mamadou, I., and Sultan, B.: What controls the isotopic composition of the African monsoon precipitation? Insights from event-based precipitation collected during the 2006 AMMA field campaign, Geophys. Res. Lett., 35, L24808, doi:10.1029/2008GL035920, 2008. 3991

Rozanski, K., Araguás-Araguás, L. J., and Gonfiantini, R.: Isotopic patterns in modern global precipitation, in: Climate Change in Continental Isotopic Records (Geophysical Monograph), edited by: Swart, P., Lohmann, K., McKenzie, J., and Savin, S., AGU, Washigton, DC, 1–36, 1993. 3991

Sachse, D., Billault, I., Bowen, G. J., Chikaraishi, Y., Dawson, T. E., Feakins, S. J., Freeman, K. H., Magill, C. R., Mclnerney, F. A., van der Meer, M. T. J., Polissar, P., Robins, R. J., Sachs, J. P., Schmidt, H.-L., Sessions, A. L., White, J. W. C., West, J. B., and Kahmen, A.: Molecular paleohydrology: interpreting the hydrogen-isotopic composition of lipid biomarkers from photosynthesizing organisms, Annu. Rev. Earth Pl. Sc., 40, 221–249, 2012. 3991

Saito, N.: On the structure of medium-scale depressions over the east China sea during AMTEX'75, J. Meteorol. Soc. Jpn., 55, 286–300, 1977. 4010

Schnider, U., Becker, A., Finger, P., Meyer-Christoffer, A., Rudolf, B., and Ziese, M.: GPCC Full Data Reanalysis Version 6.0 at 0.5°: Monthly Land-Surface Precipitation from Rain-Gauges built on GTS-based and Historic Data, doi:10.5676/DWD_GPCC/FD_M_V6_050, 2011. 4006

Sturm, C., Zhang, Q., and Noone, D.: An introduction to stable water isotopes in climate models: benefits of forward proxy modelling for paleoclimatology, Clim. Past, 6, 115–129, doi:10.5194/cp-6-115-2010, 2010. 3991

Sturm, P. and Knohl, A.: Water vapor δ^2H and δ^{18}O measurements using off-axis integrated cavity output spectroscopy, Atmos. Meas. Tech., 3, 67–77, doi:10.5194/amt-3-67-2010, 2010. 3997

Takano, I.: Analysis of an intense winter extratropical cyclone that advanced along the south coast of Japan, J. Meteorol. Soc. Jpn., 80, 669–695, 2002. 4004, 4010

Thompson, D. and Wallace, J.: The Arctic oscillation signature in the wintertime geopotential height and temperature fields, Geophys. Res. Lett., 25, 1297–1300, 1998. 4009

Thompson, D. and Wallace, J.: Annular modes in the extratropical circulation. Part I: Month-to-month variability, J. Climate, 13, 1000–1016, 2000. 4009

CPD
10, 3989–4032, 2014

Tomita, T., Yamaura, T., and Hashimoto, T.: Interannual variability of the Baiu season near Japan evaluated from the equivalent potential temperature, J. Meteorol. Soc. Jpn., 89, 517–537, 2011. 3999

Treble, P. C., Budd, W. F., Hope, P. K., and Rustomji, P. K.: Synoptic-scale climate patterns associated with rainfall δ^{18}O in southern Australia, J. Hydrol., 302, 270–282, 2005. 3992

Tremoy, G., Vimeux, F., Mayaki, S., Souley, I., Cattani, O., Risi, C., Favreau, G., and Oi, M.: A 1-year long δ^{18}O record of water vapor in Niamey (Niger) reveals insightful atmospheric processes at different timescales, Geophys. Res. Lett., 39, L8805, doi:10.1029/2012GL051298, 2012. 3991

Trenberth, K.: Recent observed interdecadal climate changes in the Northern Hemisphere, B. Am. Meteorol. Soc., 71, 988–993, 1990. 4009

Uemura, R., Matsui, Y., Yoshimura, K., Motoyama, H., and Yoshida, N.: Evidence of deuterium excess om water vapor as a indicator of ocean surface condition, J. Geophys. Res., 113, D19114, doi:10.1029/2008JD010209, 2008. 4000

Vachon, R. W., White, J. W. C., Gutmann, E., and Welker, J. M.: Amount-weighted annual isotopic (δ^{18}O) values are affected by the seasonality of precipitation: a sensitivity study, Geophys. Res. Lett., 34, L21707, doi:10.1029/2007GL030547, 2007. 3991

Vimeux, F., Tremoy, G., Risi, C., and Gallaire, R.: A strong control of the South American Seesaw on the intra-seasonal variability of the isotopic composition of precipitation in the Bolivian Andes, Earth Planet. Sc. Lett., 307, 47–58, 2011. 3991

Wang, B. and Zhang, Q.: Pacific-East Asian teleconnection. part II: How the Philippine sea anomalous anticyclone is established during El Niño development, J. Climate, 15, 3252–3265, 2002. 4009

Wang, Y. J., H., C., Edwards, R. L., An, Z. S., Wu, J. Y., Shen, C.-C., and Dorale, J. A.: A high resolution absolute-dated late Pleistocene monsoon record from Hulu cave, China, Science, 294, 2346–2348, 2001. 3991

Werle, P., Mücke, R., and Slemr, F.: The limits of signal averaging in atmospheric trace-gas monitoring by tunale diode-laser absorption spectroscopy (TDLAS), Appl. Phys. B, 57, 131–139, 1993. 3997

White, J. W. C., Barlow, L. K., Fisher, D., Grootes, P., Jouzel, J., Johnsen, S. J., Stuiver, M., and Clausen, H.: The climate signal in the stable isotopes of snow from Summit, Greenland: results of comparisons with modern climate observations, J. Geophys. Res., 102, 26425–26439, 1997. 3991

CPD
10, 3989–4032, 2014

Wu, B. and Wang, J.: Winter Arctic oscillation, Siberian high and East Asian Winter monsoon, Geophys. Res. Lett., 19, 1897, doi:10.1029/2002GL015373, 2002. 4010

Xie, S.-P., Du, Y., Huang, G., Zheng, X.-T., Tokinaga, H., Hu, K., and Liu, Q.: Decadal shift in El Niño influences on Indo-Western Pacific and east Asian climate in the 1970s, J. Climate, 23, 3352–3368, 2010. 4009

Yihui, D. and Chan, J.: The east Asian summer monsoon: and overview, Meteorol. Atmos. Phys., 89, 117–142, 2005. 3994, 3995

Yoshimura, K., Oki, T., Ohte, N., and Kanae, S.: Colored moisture analysis estimates of variations in 1998 Asian monsoon water sources, J. Meteorol. Soc. Japan, 82, 1315–1329, 2004. 3994, 3999

CPD
10, 3989–4032, 2014

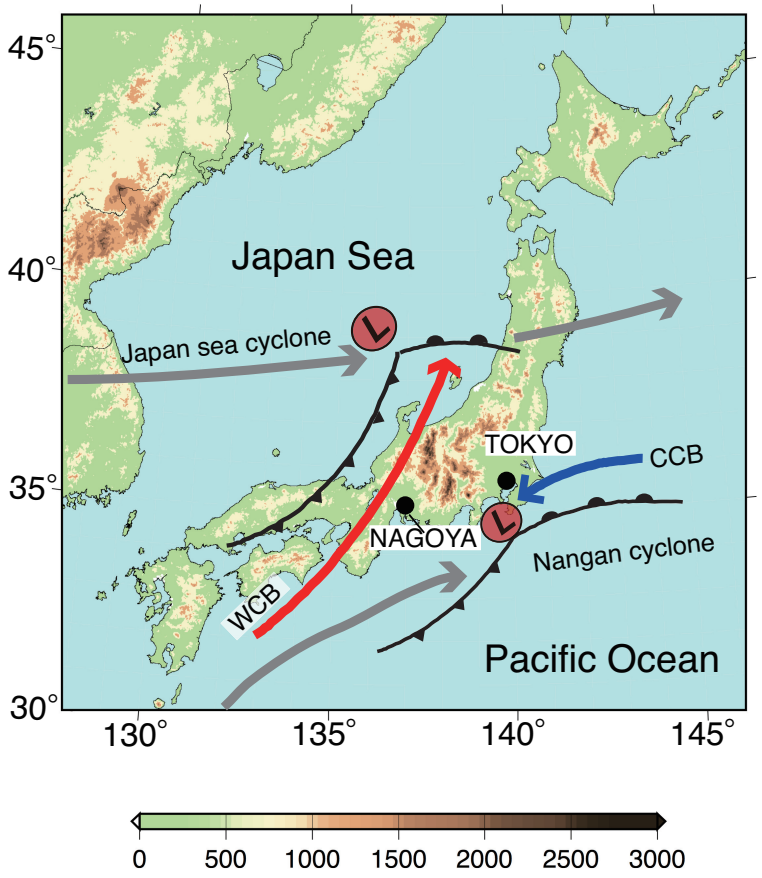

Figure 1. Topographical map of Japan showing the observation site locations (Nagoya and Tokyo). Solid gray lines represent typical cyclone tracks (Nangan cyclone and Japan Sea cyclone) over the Japan archipelago during winter. The red and blue arrows represent the warm conveyor belt (WCB), and the cold conveyor belt (CCB), respectively.

CPD
10, 3989–4032, 2014

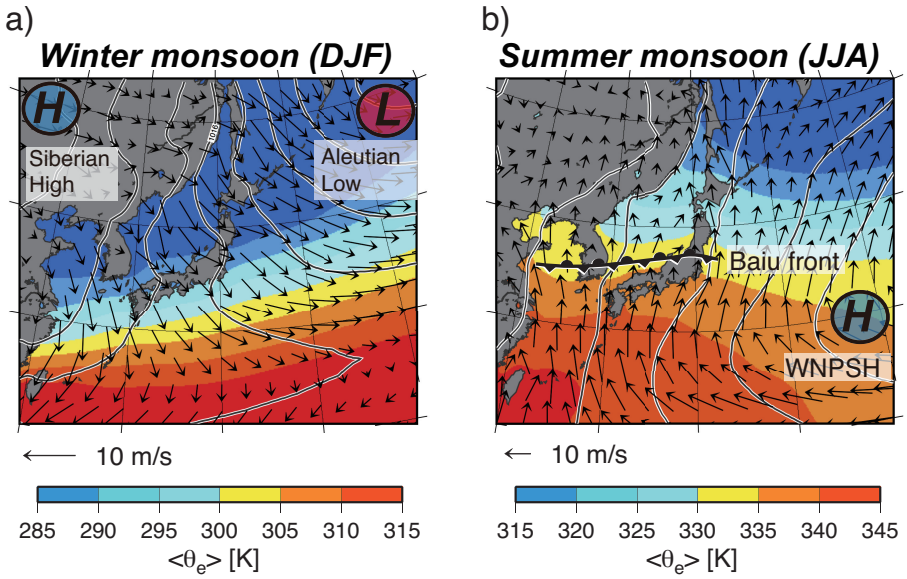

Figure 2. Seasonal mean field of vertically averaged (850–925 hPa) equivalent potential temperatures $\langle\theta_e\rangle$ (shading over the oceans: K), sea level pressure (solid contours, contour interval 4 hPa) and surface wind (vectors: m s^{-1}) for Japan region during **(a)** winter and **(b)** summer from 1961 to 1979. Symbols H and L are centers of high and low surface air pressure, respectively. The letter WNPSH represents the western North Pacific subtropical high.

CPD
10, 3989–4032, 2014

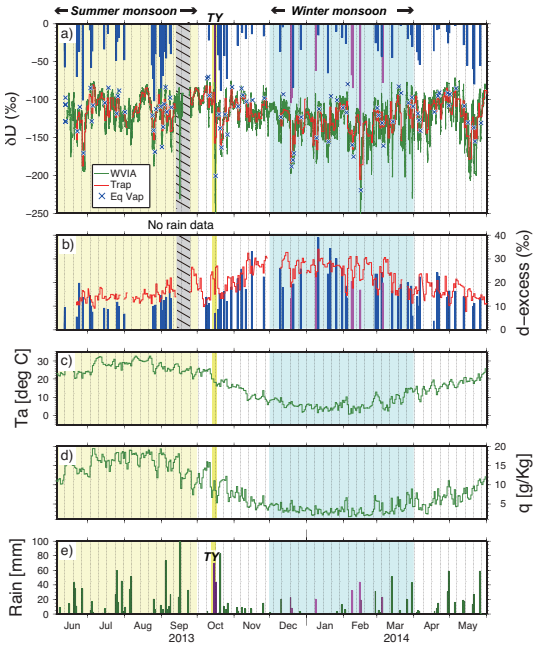

Figure 3. Time series of isotopic values and surface meteorological variables at Nagoya in Japan for the period of June 2013 to June 2014 (summer: shaded in light yellow; winter: shaded in sky-blue). **(a)** δD in precipitation (bar) and surface vapor measured by the laser instrument (green line) and by the conventional cold trap method (red line). The black cross represents the calculated δD of vapor in isotopic equilibrium with precipitation at surface air temperature. Pink-colored bars represent rainfall from Nangan cyclones. **(b)** The d-excess in precipitation and surface vapor measured by the cold trap method. **(c)** Air temperature, **(d)** mixing ratio and **(e)** precipitation observed at the nearest meteorological station. The "TY" at the top of the figure corresponds to the passage of a typhoon at the observation site.

CPD
10, 3989–4032, 2014

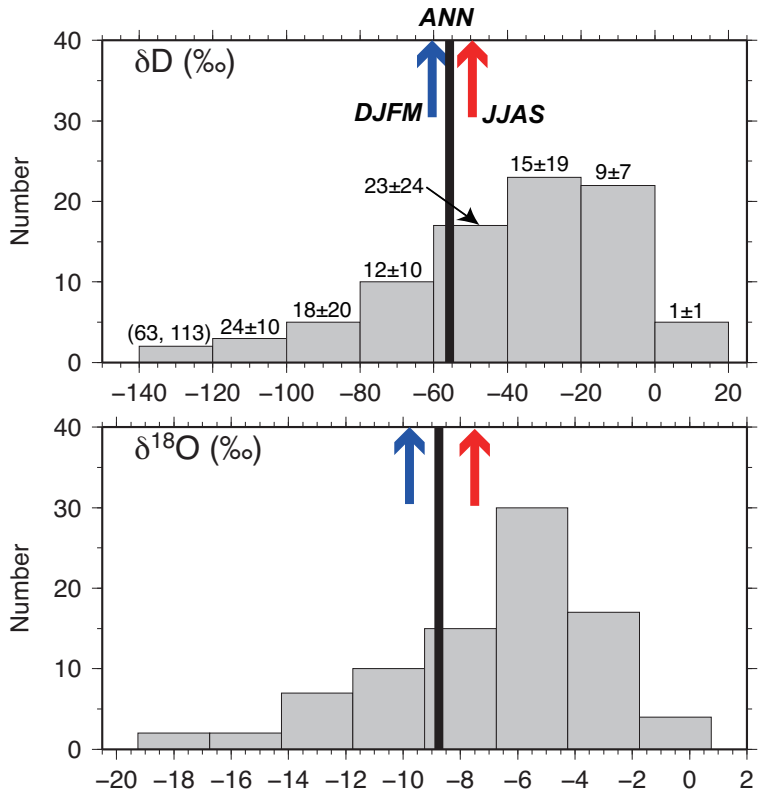

Figure 4. Histograms of (upper panel) δD and (lower panel) δ^{18}O values in event-based precipitation. The black line represents the annual mean value weighted by precipitation amount. Blue and red arrows correspond to the winter (DJFM) and summer (JJAS) mean value. The numbers on each bar in the top figure represent average precipitation amount at each bin.

CPD
10, 3989–4032, 2014

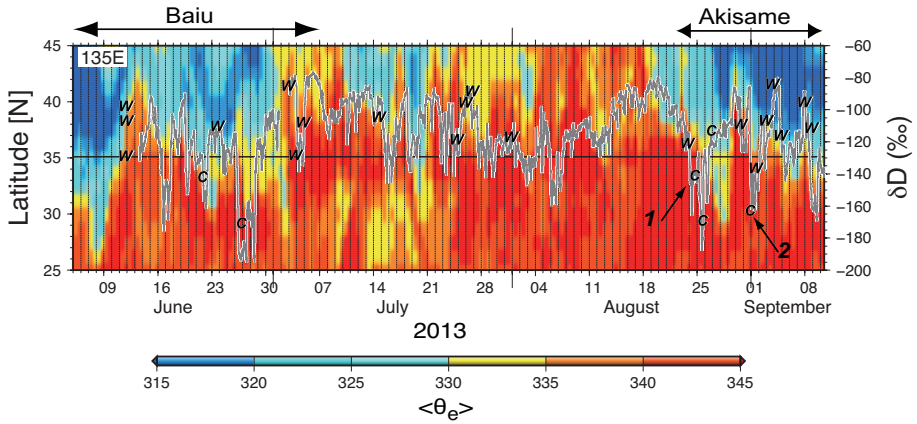

Figure 5. Time series of the value of δD in surface vapor observed at Nagoya University (gray line) and vertically averaged (850–925 hPa) equivalent potential temperatures $\langle\theta_e\rangle$ (K) between 25° N and 45° N along 135° E during summer (JJAS) in 2013. The labeled W's (C's) represent the value of δD in surface vapor in equilibrium with warm (cold) type precipitation at the same site.

CPD
10, 3989–4032, 2014

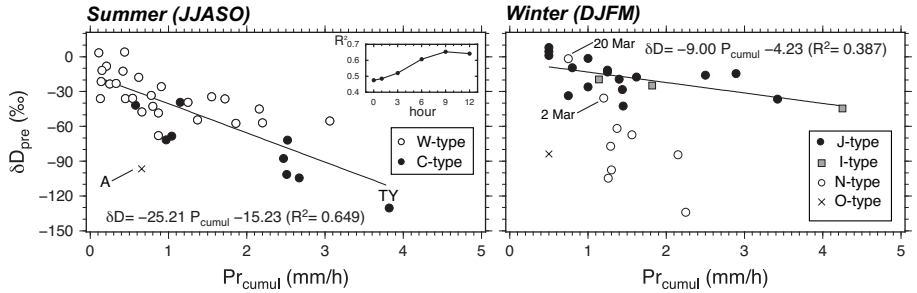

Figure 6. Relationships between δD values in individual precipitation events and cumulative precipitation amount (P_{cumul}) over nine hours back trajectories of the air mass launched from the observation site in **(a)** summer (from June to October) and **(b)** winter (December to March). Symbols indicate each different precipitation type (see detail in the text). Inset: variation in the correlation coefficient (R^2) for δD-P_{cumul} relationship with variation in the period of accumulation. The highest R^2 values were observed with nine hours of cumulative precipitation in summer.

CPD
10, 3989–4032, 2014

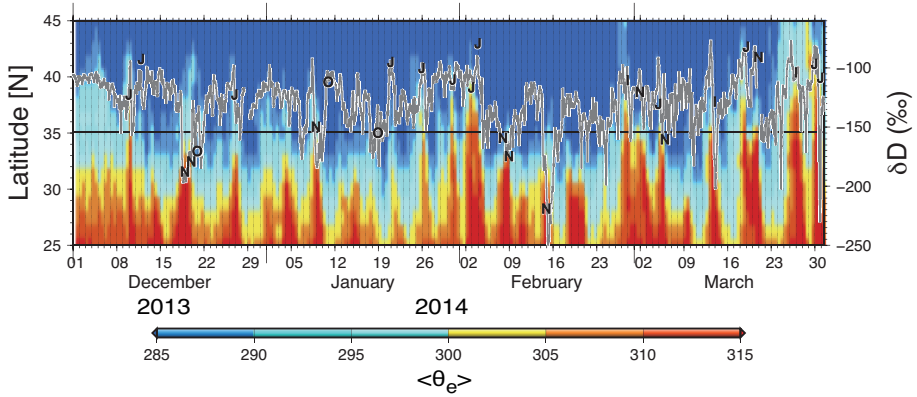

Figure 7. Same as Fig. 5, but represents the time-series for the winter (DJFM) season. The labeled characters (J, I, N, O) represent the type of precipitation event as follows: J, Japan Sea-type; I, Intermediate-type; N, Nangan-type; and O, Others-type.

CPD
10, 3989–4032, 2014

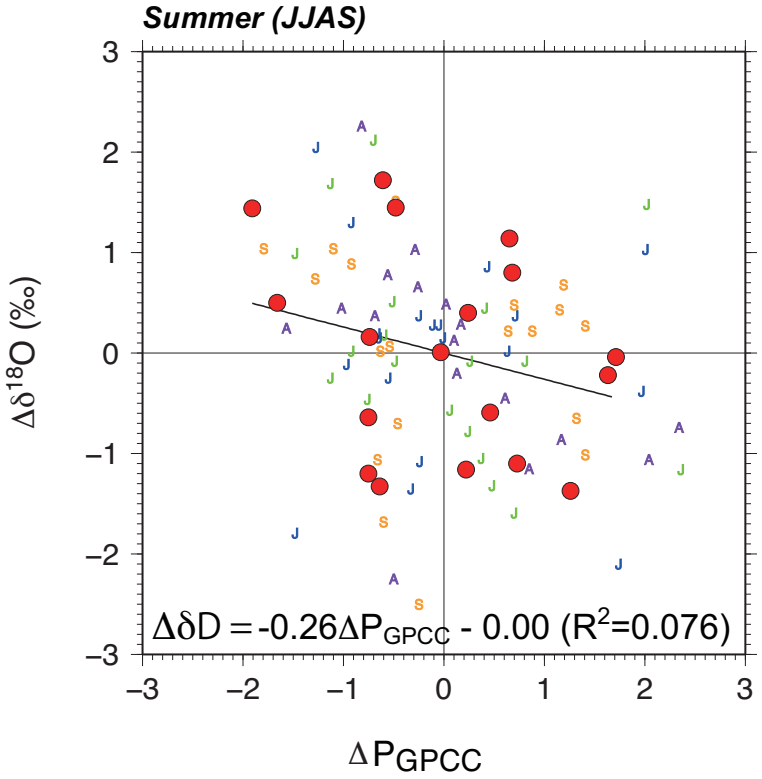

Figure 8. Anomalous plot of δ^{18}O in precipitation at GNIP Tokyo station vs. gridded precipitation derived from the GPCC (0.5° × 0.5°) at the nearest grid point to Tokyo. Anomalies for monthly and seasonal averaged δ^{18}O and precipitation were calculated by subtracting the long-term mean for that month and season and then dividing by the standard deviation. The long-term means were calculated from all available δ^{18}O records (1962–1979) at GNIP Tokyo and GPCC dataset for precipitation. Red circles represent the precipitation-weighted values in summer (from June to September).

CPD
10, 3989–4032, 2014

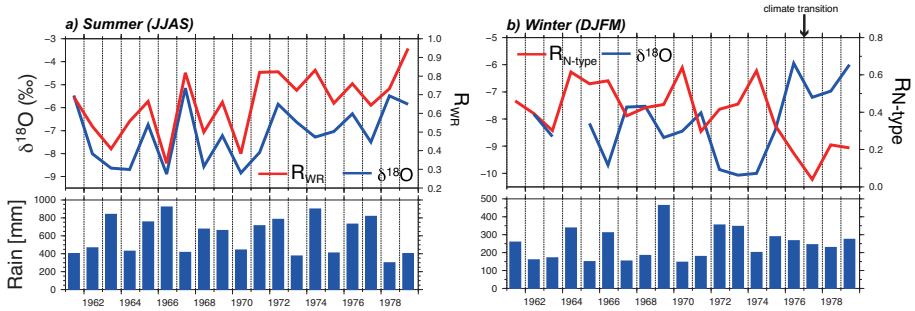

Figure 9. (a) Top: comparison of precipitation-weighted δ^{18}O in summer precipitation at Tokyo station and the ratio of the warm rainfall to the total precipitation R_{WR} for the 1961–1979 period. Bottom: the total summer precipitation amount at a meteorological station located near the GNIP Tokyo station. **(b)** Same as **(a)**, but for $R_{N\text{-type}}$.

CPD
10, 3989–4032, 2014

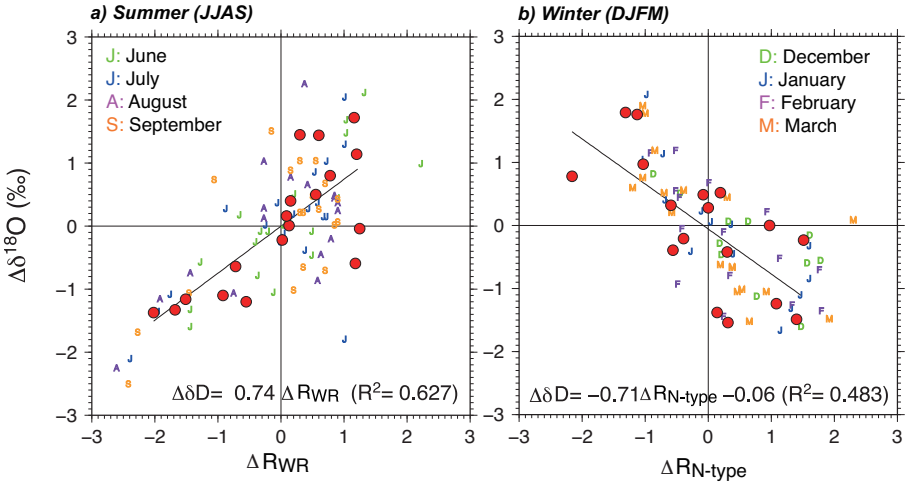

Figure 10. Same as Fig. 8. Plots **(a)** the ratio of warm rainfall to total summer precipitation (R_{WR}) and **(b)** the ratio of the Nangan precipitation ratio to the total winter precipitation ($R_{N\text{-}type}$).

CPD
10, 3989–4032, 2014

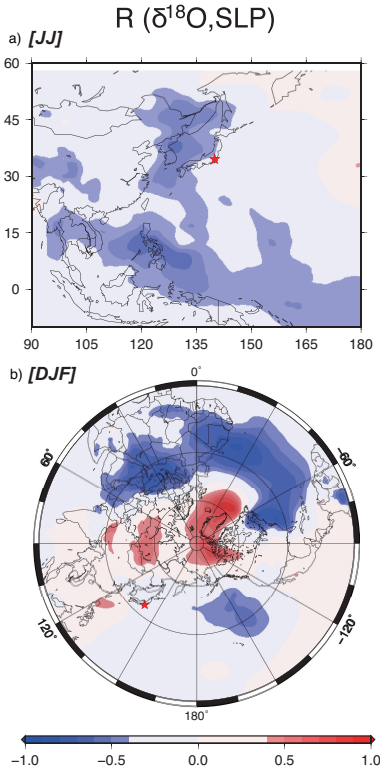

Figure 11. Correlation of the anomalies in precipitation δ^{18}O at Tokyo (red star) to SLP anomalies during **(a)** the first rainy season (June–July) and **(b)** mid winter (DJF). Color shading indicates correlations with 90 % confidence level.

CPD
10, 3989–4032, 2014

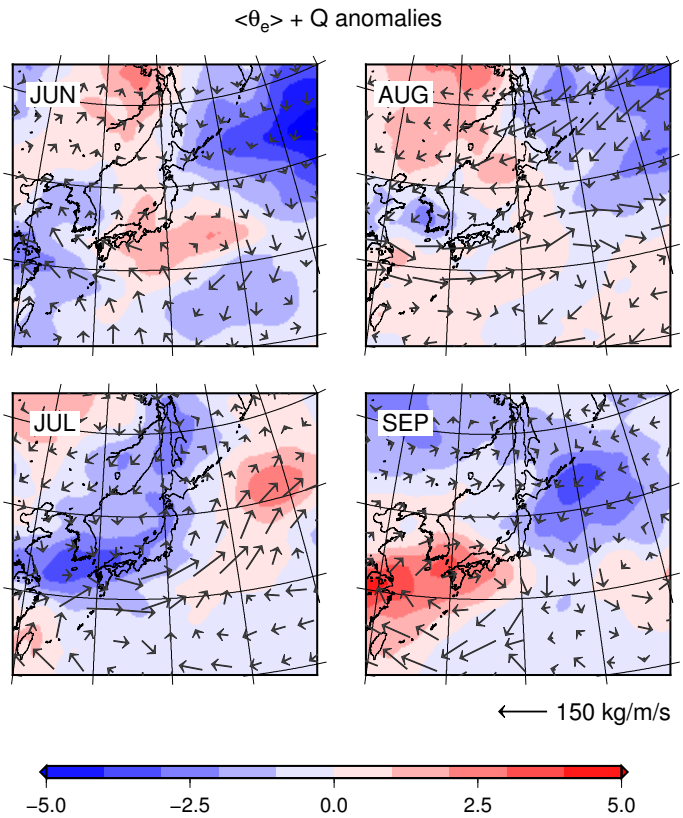

Figure 12. Composites of monthly $\langle\theta_e\rangle$ anomalies (color) and vertically integrated water vapor flux (Q) anomalies (arrow) relative to the climatology (1961–1979) for the case that summer precipitation δ^{18}O was significantly lower than the climate average (1963, 1966 and 1970).

CPD
10, 3989–4032, 2014

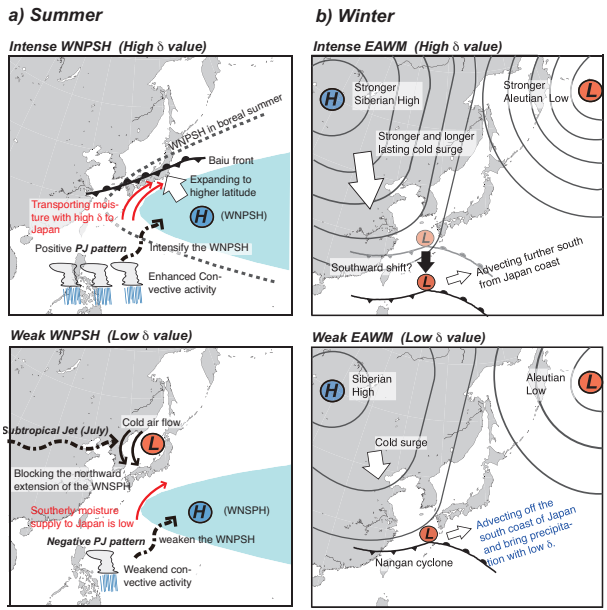

Figure 13. A schematic diagram describing the atmospheric circulation controls on the interannual variability in precipitation isotope ratio in Japan during **(a)** summer and **(b)** winter. During summer, isotopic variation in precipitation is related to the strength of the WNPSH because southwesterlies along the northwestern edge of the WNPSH transport moisture with relatively higher isotope ratio to Japan, resulting in a higher isotope ratio of precipitation. The strength of the WNPSH is influenced by the convective activity over the tropical western North Pacific (Nitta, 1987; Kosaka and Nakamura, 2006) and wave activity along the subtropical jet (Enomoto, 2003). On the other hand, isotopic values in winter precipitation reflect the EAWM activity (cold surge) which influence the genesis or the tracks of Nangan cyclones, bringing cold precipitation with lower isotopic values to central Japan. The EAWM is intensified (weakened) during the negative (positive) phase of the Arctic Oscillation. See text for more detail.

CPD
10, 3989–4032, 2014